JURNAL UPI

ASEAN Journal of Science and Engineering

AJSE
ASEAN Journal of Science and Engineering

Journal homepage: http://ejournal.upi.edu/index.php/AJSE/

Standardized Assessment of Compressive Behavior in Rigid Polyurethane Foams: Influence of Density, Crosslinking, and Aging

Harith H. Al-Moameri [*1, 2], *Sarmad Al-Anssari* [2,3], *Ali Abed Salman* [1], *Arnold A. Lubguban* [4], *Gerard G. Dumancas* [5]

[1]Mustansiriyah University, Baghdad, Iraq
[2]Al-Naji University, Baghdad, Iraq
[3]Baghdad University, Baghdad, Iraq
[4]Mindanao State University-Iligan Institute of Technology, Iligan, the Philippines
[5]North Carolina Agricultural and Technical State University, Greensboro, NC, United States

*Correspondence: E-mail: almoamerih@uomustansiriyah.edu.iq; almoamerih@alnaji-uni.edu.iq

ABSTRACT

Rigid polyurethane foams (RPUFs) are essential materials in structural applications due to their thermal insulation, lightweight properties, and mechanical strength. However, evaluating and comparing their compressive performance is complicated by differences in formulation parameters such as density, aging, and crosslink density. This study proposes a standardized normalization approach to evaluate compressive properties across diverse RPUF formulations by adjusting all data to a common reference density. Samples were subjected to controlled aging conditions and analyzed using dynamic mechanical thermal analysis (DMTA) to investigate the relationship between crosslinking behavior and mechanical performance. The results demonstrate that aging, formulation composition, and isocyanate index significantly influence the foam's compressive strength and modulus, as well as its thermal transitions. The proposed method enables a more reliable and efficient comparison of RPUF performance, offering practical implications for optimizing formulation design in construction, automotive, and aerospace applications where mechanical integrity and durability are critical.

ARTICLE INFO

Article History:
Submitted/Received 20 May 2025
First Revised 26 Jul 2025
Accepted 03 Sep 2025
First Available online 04 Sep 2025
Publication Date 01 Mar 2026

Keyword:
Building material,
Compressive behavior,
Crosslinking density,
Normalization approach,
Polyurethane,
Polyurethane aging.

1. INTRODUCTION

Plastics have become a ubiquitous class of materials in contemporary industries because of their adaptability, affordability, and processability. Numerous reports on plastic have been published [1-4]. With their derivation largely from petrochemical sources, plastics encompass a diverse spectrum of polymer types, each specifically developed for targeted properties of mechanics, heat, and chemical resistance. Their lightweight, coupled with the robustness and flexibility of product designs, has led to their universal usage across industries such as packaging, construction, vehicles, electronics, and healthcare. However, the growing global usage of plastics has led to increased concerns over their environmental sustainability, largely because of their non-biodegradability and role in contributing to lingering pollution over time. In response to these issues, recent studies have focused on developing enhanced functionality of plastic materials with advanced formulations, functional additives, and hybrid composites while looking into other substitutes such as bio-based or recoverable polymers. Among these, polyurethane systems (particularly foams) have drawn interest for their structural functionality and insulating abilities, and they are of intense focus in developing high-performance and more environmentally sustainable plastic usage.

Low-density rigid polyurethane foams (RPUFs) are popular, cost-effective, and efficient insulations that are applied in numerous industries, such as residential and commercial buildings, industrial processes, and transportation systems [5]. The most typical ones include wall and roof insulation, gap sealing with spray foam, refrigeration units, and structural reinforcement with sandwich panels [6]. The high usage of RPUFs can be attributed to the combination of desirable traits, such as low thermal conductivity, lightweight composition, mechanical strength, and versatility in various shapes, such as sprayed or molded structures [7–9]. Their closed-cell structure reduces heat loss through the entrapment of blowing agents, and their resistance to moisture and stability in terms of shape and size with changes in environmental conditions contribute to improved performance [10–17].

In practical settings, RPUFs frequently endure compressive loads during storage, transportation, or service life, particularly in scenarios such as roofing, where foot traffic imposes mechanical stress [18–20]. The compressive strength of polyurethane foam, defined as the maximum stress sustained before or at 10% deformation, plays a critical role in determining its suitability for such applications. Compression initially causes the polymer matrix to deform, followed by cell wall contact and densification as loading progresses [9, 21–23].

Assessing compressive properties in three orthogonal directions typically requires large, well-machined foam samples and complex testing protocols [24]. These directional strengths are geometrically averaged and normalized to a reference density to isolate the influence of formulation variables on mechanical performance. While effective, this approach is cumbersome and inefficient, particularly in product development contexts where rapid screening of formulations is necessary [25–28].

Foam density is among the most influential parameters affecting compressive behavior [13, 20]. Due to its strong correlation with mechanical strength, normalization to a consistent density is essential for meaningful comparison between formulations. Additional factors such as foam age, cell morphology, and chemical composition also contribute to variability in compressive properties [29–31].

Aging further complicates performance evaluation by inducing chemical and structural changes over time [32–35]. Various degradation mechanisms—such as oxidation, hydrolysis, thermal exposure, ultraviolet radiation, loss of plasticizers, microcracking, crosslinking imbalances, and moisture absorption—alter the foam's internal structure and reduce its

DOI: https://doi.org/10.17509/ajse.v6i1.89937
p- ISSN 2776-6098 e- ISSN 2776-5938

ability to withstand compressive forces [36–39]. While some foams may temporarily benefit from post-curing crosslinking, the overall trend typically involves progressive decline in strength due to material embrittlement and network deterioration [40–42].

Despite recognition of these variables, a significant research gap persists in the form of a missing standardized, efficient method for evaluating compressive properties across different RPUF formulations. Conventional methods are labor-intensive and ill-suited for rapid prototyping or high-throughput optimization. Moreover, the combined effects of foam density, aging, crosslink density, and isocyanate index under controlled conditions remain insufficiently understood.

Therefore, this study aims to develop a simplified normalization method that enables fair, efficient, and systematic comparison of compressive strength and modulus across various RPUF formulations by adjusting data to a uniform density. The study also seeks to evaluate the individual and combined effects of aging, crosslink density, and isocyanate index on mechanical performance. By integrating dynamic mechanical thermal analysis (DMTA) into this framework, the research contributes a practical and scalable approach for optimizing RPUF formulations, with direct relevance to industries demanding durable, load-bearing, and thermally efficient materials.

2. METHODS

2.1. Materials and Foam Preparation

The RPUF formulations were prepared using 100 grams of JEFFOL 393 polyol (designated as Jeff 1) and polymeric methylene diphenyl diisocyanate (PMDI), both obtained from Huntsman Company. All formulations maintained a constant isocyanate index of 1.1. Distilled water (1 g) was used as the chemical blowing agent. **Table 1** summarizes the key properties of the polyols and PMDI.

The RPUF formulations were prepared using 100 grams of JEFFOL 393 polyol (designated as Jeff 1) and polymeric methylene diphenyl diisocyanate (PMDI), both obtained from Huntsman Company. All formulations maintained a constant isocyanate index of 1.1. Distilled water (1 g) was used as the chemical blowing agent. **Table 1** summarizes the key properties of the polyols and PMDI.

Table 1. Specifications of polyols and PMDI.

Property	Jeff 1	Jeff 2	Jeff 3	PMDI
Specific gravity (@25°C)	1.08	1.06	1.07	1.19
Functionality	3.9	3.2	3.0	2.72
Hydroxyl number (mgKOH/g)	393	310	635	–
Water content (%)	0.1	0.1	0.1	–
NCO content (wt%)	–	–	–	31.2
Viscosity (cP @ 25°C)	5000	2200	430	156–216

The B-side components (comprising polyol, catalysts, surfactant, and nanoparticles) were thoroughly mixed in a plastic container and subsequently blended with PMDI for 10 seconds using a mixer blade operating at 2000 rpm, mounted on a table drill press [43]. The resulting mixture was immediately poured into a wooden mold (11 × 11 cm^2), lined with aluminum foil to prevent adhesion. The exothermic polymerization reaction induced foam expansion, with the reaction temperature monitored using a Reed SD-947 Data Logger. The foaming process was considered complete once the temperature began to decline, indicating stabilization of the polymer network [44].

DOI: https://doi.org/10.17509/ajse.v6i1.89937
p- ISSN 2775-6793 e- ISSN 2775-6815

To establish a testing methodology, foams were produced at nine different density levels (R1-1 through R1-9) by varying the amount of physical blowing agent (cyclopentane), as presented in **Table 2**. Key parameters, including cell morphology, density, and aging behavior, were analyzed.

Table 2. Amount of physical blowing agent (PBA) for different foam formulations.

Foam Sample	PBA (g)
R1-1	4
R1-2	6
R1-3	8
R1-4	10
R1-5	12
R1-6	14
R1-7	16
R1-8	18
R1-9	20

Following the optimization of foam density methodology, additional formulations were fabricated to examine the effects of crosslink density (recipes R2-1 to R2-4) and isocyanate index (recipes R3-1 to R3-5). All foam samples were stored untrimmed at 25°C until testing, with storage durations varied according to subsequent experimental procedures.

2.2. Cell Size Analysis

To evaluate structural anisotropy, foam samples were analyzed for variations in cell size and orientation, which are critical in determining compressive performance. Samples were extracted from the uppermost region of each foam block. Average cell dimensions were measured along both the rise direction and perpendicular to it to capture anisotropy. Measurements were conducted using an RM 5 Raman microscope (Leica S/N 255150 BZ 03) coupled with an ELMO CCTV digital signal processing camera. A magnification of 500 µm was used to capture detailed cellular structure [45–47].

2.3. Compressive Testing

Compressive tests were performed on foam specimens cut to dimensions of 5.8 × 5.08 × 2.54 cm, taken from the upper portion of each foam block. Before testing, all samples were conditioned at 25°C for 24 hours. Tests were conducted in the rise direction in accordance with ASTM D1621 standards. Each sample was tested in triplicate, and the average value was reported for analysis [48–50].

2.4. Crosslink Density Characterization

Crosslink density was evaluated using the equilibrium swelling method based on the Flory–Rehner equation [40, 51–53]. Foam samples were cut into small, uniform pieces. The initial dry mass (m_d) and density (ρ_d) were recorded. Samples were immersed in toluene until the swelling equilibrium was achieved. The swollen mass (m_s) was then recorded after surface blotting. Finally, samples were dried and weighed again to ensure mass consistency. The polymer volume fraction in the swollen samples (v_r) was calculated using Equation (1).

$$v_r = \frac{Voluem\ of\ the\ polymer}{Total\ volume\ of\ the\ swollen\ samples} = \frac{m_d/\rho_d}{m_s/\rho_s} \quad (1)$$

where ρ_d and ρ_s are the densities of the dry and swollen foam samples, respectively.

DOI: https://doi.org/10.17509/ajse.v6i1.89937
p- ISSN 2776-6098 e- ISSN 2776-5938

The crosslink density (μμ) was determined using the Flory–Rehner correlation (Equation (2)).

$$\mu = -\frac{[ln(1-v_r)+v_r+\chi*v_r^2]}{\left[V_0*\left(v_r^{1/3}-\frac{v_r}{2}\right)\right]} \quad (2)$$

Here, V_0 is the molar volume of toluene (106.8 cm³/mol), and χ is the Flory–Huggins interaction parameter, given by Equation (3).

$$\chi = 0.35 + \frac{V_0}{RT}(solubility\ of\ toluene - solubility\ of\ sample) \quad (3)$$

2.5. Dynamic Mechanical Analysis (DMA)

Rectangular foam specimens (0.5 × 1 × 5 cm) were cut from the center of the free-rise region. All samples were free of surface contaminants. Dynamic mechanical analysis was performed using a Physical MCR301 rheometer (Anton Paar) equipped with a solid torsion fixture under a nitrogen atmosphere.

A small oscillatory force was applied to the samples while the temperature was increased from 50°C to 250°C at a rate of 3°C/min, with a frequency of 1 Hz. The DMA recorded changes in storage modulus, loss modulus, and tan δ as functions of temperature. The glass transition temperature (*Tg*) was identified either by the peak in the tan δ curve or by a distinct drop in the storage modulus [54-56].

3. RESULTS AND DISCUSSION

3.1. Effect of Foam Density

Foam density was systematically varied by adjusting the loading of the physical blowing agent (cyclopentane). To assess how density governs cell geometry and compressive response, specimens were taken from the core region of each block near the mold wall (box edge), where processing gradients are minimal and microstructure is representative. **Figure 1** presents optical micrographs (RM 5 Raman microscope used in optical imaging mode with a DSP camera) of the cell morphology in the two principal directions: (i) the normal (perpendicular) to the rise direction and (ii) the parallel to the rise direction. In **Figure 1(a)**, cells appear more equiaxed and compact, a morphology that promotes uniform stress transfer under compressive loading normal to the rise. In **Figure 1(b)**, cells are visibly elongated along the rise axis, reflecting the kinematics of foam expansion and gas escape during foaming; this elongation imparts greater compliance and energy-dissipation capacity for loads applied parallel to the rise.

Quantitatively, the measured average cell sizes fall in the range 0.55-0.61 mm in the normal direction and 0.67-0.73 mm in the parallel direction, yielding a stable anisotropy ratio of 1.2 across the density series (see Equation (4)). This relatively constant anisotropy indicates that changes in compressive properties with density are driven primarily by cell size/solid fraction rather than by directional changes in cell shape. Consistent with cellular solids theory, the smaller, more equiaxed cells in the normal direction enhance load-bearing capacity, whereas the elongated cells parallel to the rise contribute to strain accommodation and resilience during deformation.

$$Cell\ Anisotropy\ Ratio = \frac{Dimension\ in\ the\ rise\ direction}{dimension\ perpendicular\ to\ the\ rise\ direction} \quad (4)$$

Because the anisotropy ratio is approximately constant, the geometric mean of compressive strength for an axisymmetric cellular structure can be estimated from the rise direction value; for an anisotropy ratio of 1.2, this mean is about 86% of the compressive strength measured in the rise direction. On this basis, to streamline the test matrix while preserving fidelity, subsequent compressive characterization in this study was performed in

DOI: https://doi.org/10.17509/ajse.v6i1.89937
p- ISSN 2775-6793 e- ISSN 2775-6815

the rise direction only, with the understanding that the measured trend reflects the bulk (direction-averaged) behavior with high fidelity.

Finally, the microstructural trends in **Figure 1(a)** and **(b)** align with the macroscopic density–strength relationship discussed later: as cyclopentane loading increases (reducing density), cell walls thin and cells enlarge, leading to a monotonic decrease in compressive strength. Over the examined density window, this dependence is well captured by a linear fit (high R2R^2), which we adopt for density normalization in subsequent sections to isolate formulation effects from density.

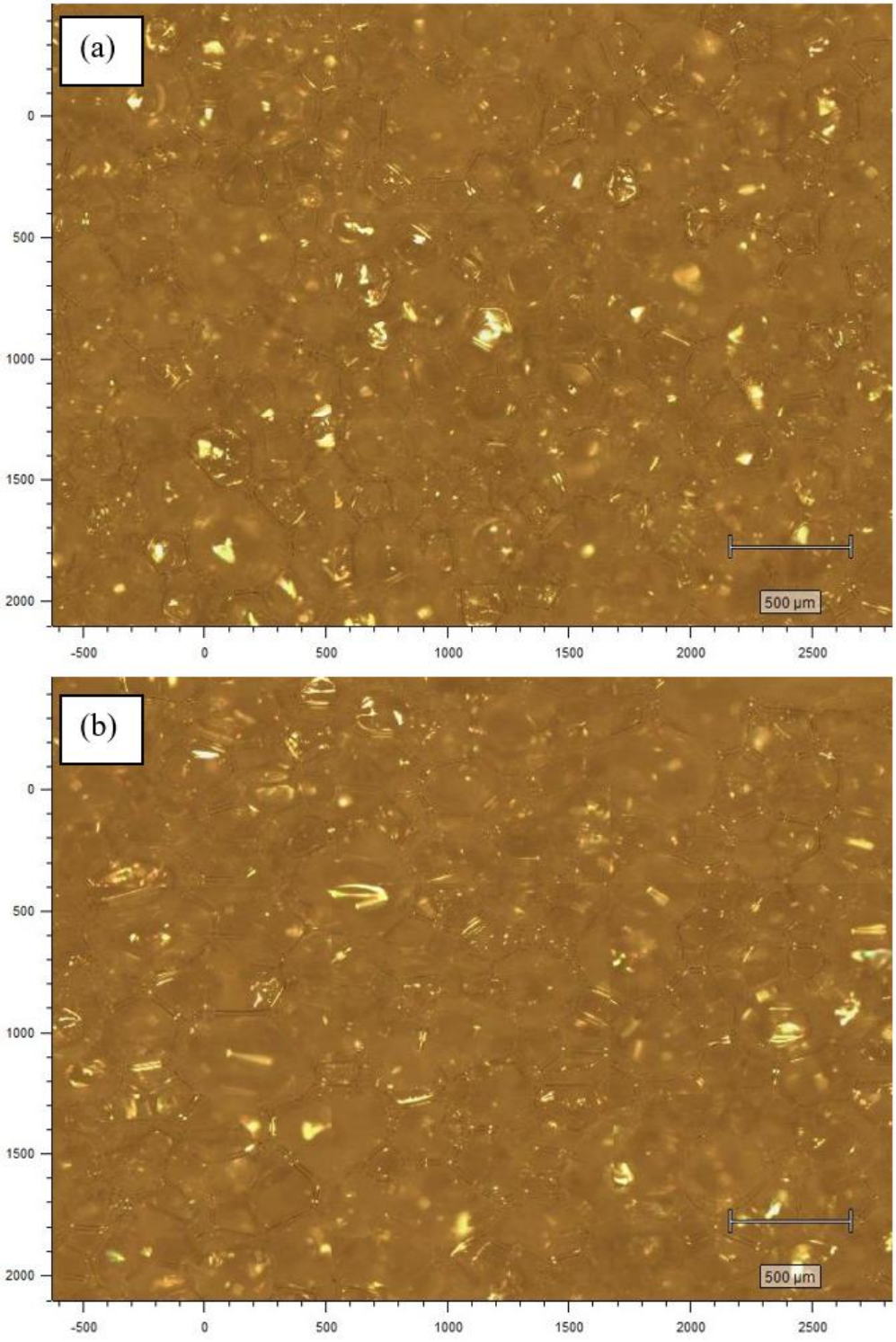

Figure 1. Cell Morphology in a) normal and b) parallel foam rise direction.

DOI: https://doi.org/10.17509/ajse.v6i1.89937
p- ISSN 2776-6098 e- ISSN 2776-5938

For axisymmetric foams, the geometric mean of compressive strength can be approximated based on the observed cell anisotropy ratio [2]. When the anisotropy ratio is approximately 1.2, as identified in this study, the geometric mean compressive strength is estimated to be around 86% of the compressive strength measured in the rise direction. Given the uniformity in cell morphology across all samples (regardless of blowing agent level), this approximation provides a reliable basis for simplifying the experimental methodology. As such, compressive testing was conducted only in the rise direction, allowing for consistent, efficient evaluation of mechanical performance while minimizing experimental complexity.

Figure 2 presents the foam densities achieved at nine different levels of cyclopentane loading, corresponding to formulations R1-1 through R1-9. The plotted error bars represent the standard deviations from three replicate measurements, reflecting the reproducibility of foam density at each blowing agent level. As expected, an inverse relationship was observed between cyclopentane loading and foam density, consistent with increased gas expansion and lower polymer content. However, beyond a certain threshold (specifically at the two highest blowing agent levels (R1-8 and R1-9)), further increases in cyclopentane did not result in additional decreases in density. This suggests that the foam system had reached its expansion limit, likely constrained by factors such as polymer network strength, surface tension, and gas escape during foaming. In some cases, excessive blowing agent can even lead to cell coalescence or collapse, producing structurally unstable or non-uniform foams.

To ensure reliability and consistency in subsequent mechanical analysis, samples R1-8 and R1-9 were excluded from further testing. Their inclusion could introduce variability unrelated to formulation intent, obscuring the interpretation of density-dependent trends. The remaining seven formulations (R1-1 through R1-7) exhibited well-behaved and linearly correlated density variations, forming the basis for the compressive strength and modulus analysis presented in the following sections.

Figure 3 illustrates the relationship between compressive strength and foam density for the formulations R1 1 through R1 7, corresponding to the range of cyclopentane loadings that produced structurally stable foams. While compressive strength in cellular solids is typically modeled using a power-law relationship, such modeling assumes a wide range of density variations and often requires log-transformed data. In this study, however, the density range was relatively narrow (between 58 kg/m³ and 27.3 kg/m³), and the data exhibited strong linear behavior within this window.

Figure 3 illustrates the relationship between compressive strength and foam density for the formulations R1 1 through R1 7, corresponding to the range of cyclopentane loadings that produced structurally stable foams. While compressive strength in cellular solids is typically modeled using a power-law relationship, such modeling assumes a wide range of density variations and often requires log-transformed data. In this study, however, the density range was relatively narrow (between 58 and 27.3 kg/m³), and the data exhibited strong linear behavior within this window.

A linear regression model was applied, yielding an exceptionally high coefficient of determination ($R^2 = 0.9989$), which confirms the robustness of the linear fit. This high level of correlation justifies the adoption of a linear model over more complex non-linear approach. The simplicity and accuracy of this model make it especially suitable for density normalization, a core objective of this research, as it allows for straightforward correction and comparison of compressive strength across samples with different densities.

To ensure coverage of densities relevant to a wide array of practical RPUF applications, three levels of cyclopentane loading (10, 12, and 14 g) were selected for replication across all experimental recipes. This design ensured the repeatability of density influence while

DOI: https://doi.org/10.17509/ajse.v6i1.89937
p- ISSN 2775-6793 e- ISSN 2775-6815

controlling for formulation-specific effects. Consequently, the observed trend in compressive strength reflects not only the influence of density itself but also establishes a reliable framework for normalizing mechanical data, thereby enabling equitable comparisons among foam samples produced under varying conditions.

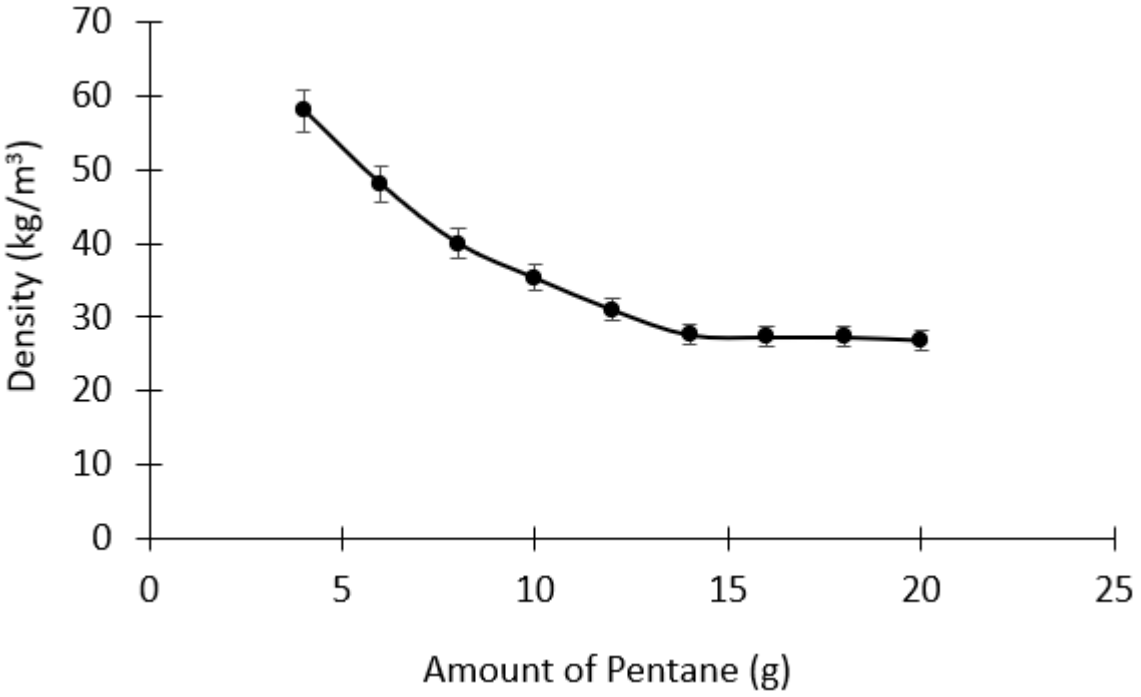

Figure 2. Foam density at different physical blowing agents.

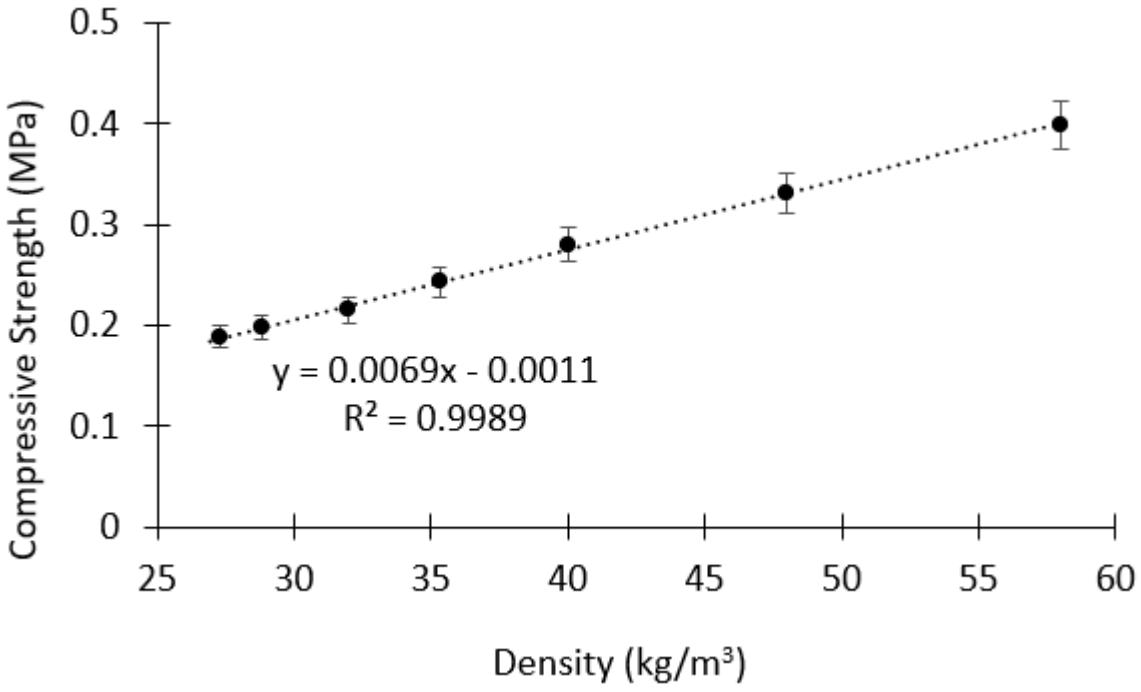

Figure 3. Impact of foam density on foam compressive strength.

DOI: https://doi.org/10.17509/ajse.v6i1.89937
p- ISSN 2776-6098 e- ISSN 2776-5938

3.2. Effect of Foam Age

To investigate the effect of short-term aging on the mechanical properties of rigid polyurethane foams (RPUFs), samples produced using five different cyclopentane loadings (formulations R1-3 to R1-7) were subjected to controlled aging conditions of 50% relative humidity and 24°C. The untrimmed foam blocks were stored for various durations (2, 6, 8, 14, and 21 days) before testing, to capture the early evolution of mechanical behavior resulting from post-curing and environmental exposure.

Compressive strength and compressive modulus were both evaluated as functions of foam density across the different aging periods, and the results are presented in **Figures 4** and **5**, respectively. It was noted that even within the same cyclopentane formulation, foam densities exhibited minor fluctuations over time. These variations may be attributed to slight changes in mass loss, gas diffusion, or polymer relaxation during aging.

To allow for an equitable comparison of mechanical properties over time, a density normalization procedure was applied to each data set. This ensured that compressive properties could be compared on a common basis, independent of density fluctuations. For each aging period, a linear regression was performed to correlate compressive strength and modulus with foam density. The resulting fitting equations for each time point are summarized in **Table 3**.

As anticipated, the analysis indicated that the compressive strength gradually increased with the density of the foam, irrespective of the aging time. This pattern is consistent with the overall reasoning that denser foams have thicker cell walls and a higher percentage of solid forms, which leads to better load-bearing properties.

Similarly, the compressive modulus exhibited a positive relationship with density throughout all aging periods. They could have done this by applying linear normalization so that the effect of aging, as opposed to confounding factors, including density, was isolated. This method provides better insight into how the intrinsic mechanical behavior of the foam matrix changes with time owing to the aging process. The normalized data are further analyzed in the following sections to measure the changes in compressive strength and modulus with respect to aging time.

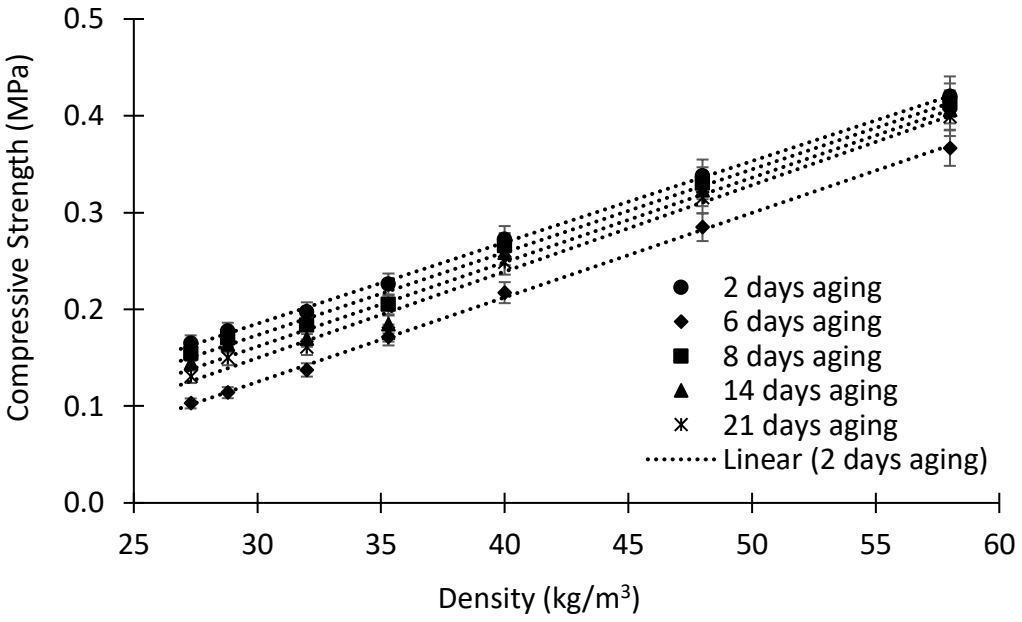

Figure 4. Impact of foam aging on foam compressive strength with different foam densities.

DOI: https://doi.org/10.17509/ajse.v6i1.89937
p- ISSN 2775-6793 e- ISSN 2775-6815

In this study, a target density of 40 kg/m³ was selected as the reference point for normalizing all compressive strength and modulus data. This normalization allows for meaningful comparisons between foam samples that may vary in density due to formulation or processing, by effectively isolating the effects of aging and formulation variables from those of density.

Using the regression equation derived from the 2-day aging data set (Equation (5)), with R^2 = 0.9989, the normalized compressive strength at 40 kg/m³ was calculated to be 0.272 MPa:

$$Compressive\ Strength\ (MPa) = 0.0084\ x\ Foam\ density\ \left(\frac{kg}{m^3}\right) - 0.0668 \quad (5)$$

The same normalization approach was applied across all aging intervals to evaluate how compressive strength and modulus evolve at a fixed density. This method ensures that observed changes in mechanical behavior reflect intrinsic aging effects, rather than variations in foam density.

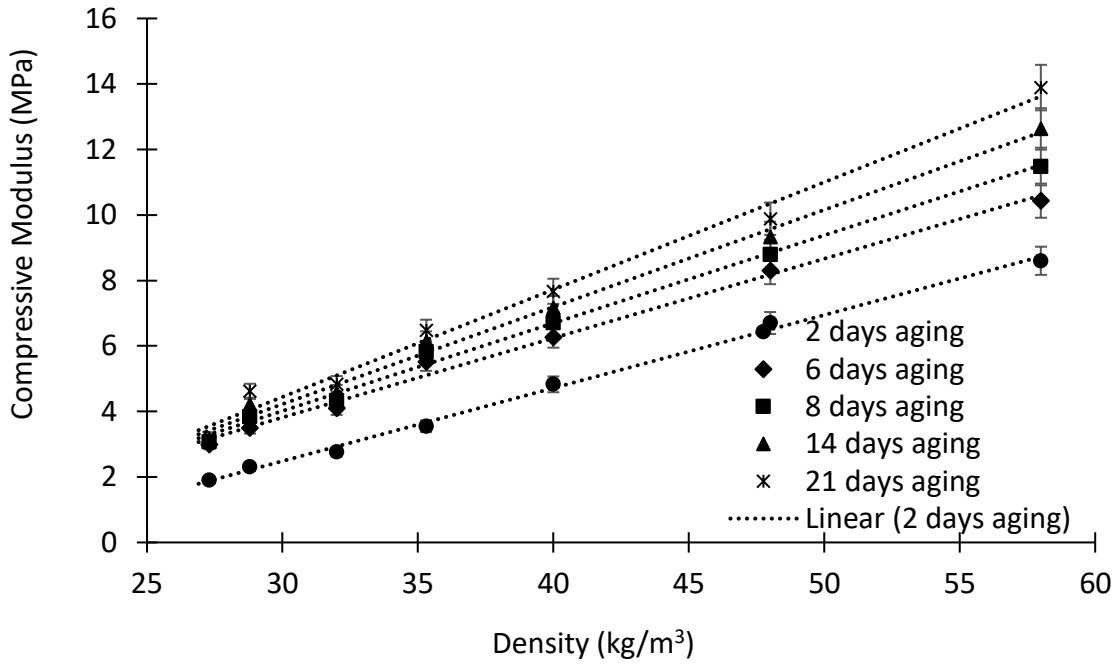

Figure 5. Impact of foam aging on foam compressive modulus with different foam densities.

Table 3. Fitting equations for the compressive strength (**Figure 4**) and compressive modulus (**Figure 5**) at different aging periods.

Aging Days	Fitting Equation	R^2 value
Compressive Strength		
2	y = 0.0084x - 0.0668	0.9989
6	y = 0.0087x - 0.1369	0.9988
8	y = 0.0089x - 0.1536	0.9954
14	y = 0.0091x - 0.1703	0.9978
21	y = 0.0093x - 0.1882	0.9966
Compressive Modulus		
2	y = 0.2231x - 4.2097	0.9967
6	y = 0.2423x - 3.4521	0.9936
8	y = 0.2682x - 4.0314	0.995
14	y = 0.2966x - 4.6761	0.9933
21	y = 0.3279x - 5.3928	0.9891

DOI: https://doi.org/10.17509/ajse.v6i1.89937
p- ISSN 2776-6098 e- ISSN 2776-5938

The results of the normalization procedure are presented in **Figures 6** and **7**, which display the evolution of compressive strength and modulus, respectively, across the aging period. Error bars represent the average standard deviation across all tested formulations, accounting for variability due to formulation and measurement.

Analysis of the normalized compressive strength revealed notable fluctuations between days 2 and 8, with the most pronounced decrease observed at day 6. These fluctuations may be attributed to changes in the gas composition within the foam cells, including the replacement of blowing agents with ambient air, diffusion-related shrinkage, or polymer relaxation during post-curing.

Over this period, the normalized compressive strength exhibited an overall decline, while the normalized compressive modulus increased significantly, suggesting a transition in foam behavior from a softer, more ductile state to a stiffer, more rigid network. This could reflect progressive crosslinking or structural reorganization at the polymer matrix level.

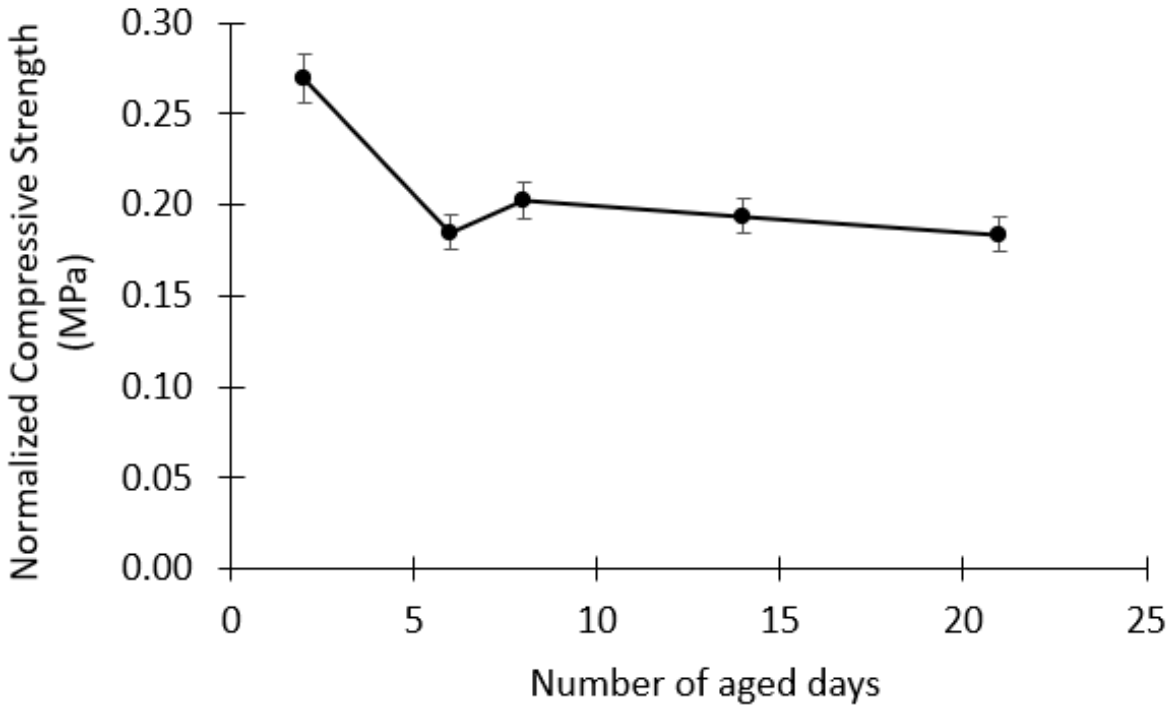

Figure 6. Normalized compressive strength over an aging period.

From day 8 onward, both the compressive strength and modulus demonstrated minimal variation, indicating that the foam had reached a relatively stable mechanical state. Based on this stabilization, all subsequent compressive testing in the study was conducted on foams aged between 8 and 21 days, to ensure data consistency and reliability across different experimental conditions.

3.3. Effect of Crosslink Density

The influence of crosslink density on the mechanical behavior of rigid polyurethane foams (RPUFs) was systematically investigated using formulations R2-1 through R2-4, as outlined in **Table 4**. These formulations were designed by varying the average functionality of the polyol blends (from 3.9 to 3.13) to induce changes in network crosslinking, while maintaining a constant hydroxyl number of 393 mgKOH/g across all blends. This ensured that differences in

DOI: https://doi.org/10.17509/ajse.v6i1.89937
p- ISSN 2775-6793 e- ISSN 2775-6815

mechanical response could be attributed primarily to crosslink density, rather than overall reactivity or chain length.

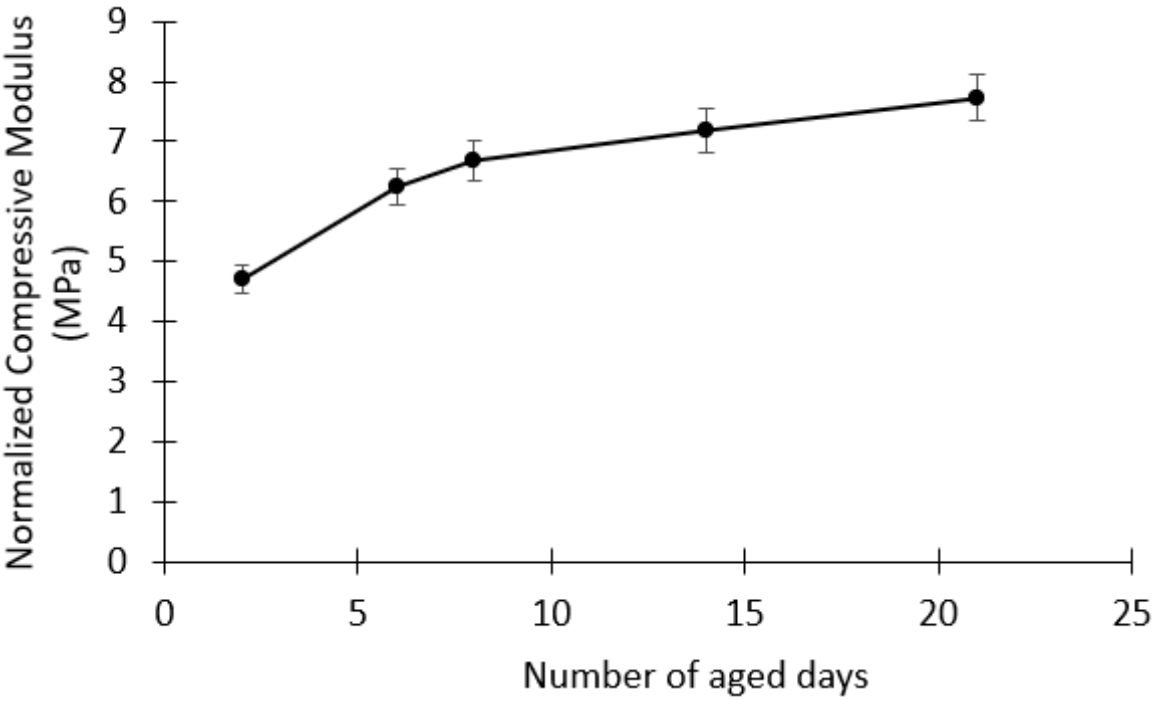

Figure 7. Normalized compressive modulus over an aging period.

Table 4. Recipes for the %relative crosslinked density.

Recipes	Foam samples			
	R2-1	**R2-2**	**R2-3**	**R2-4**
Jeff 1	100	60	30	0
Jeff 2	0	28.4	33.6	39.5
Jeff 3	0	15.7	43.4	54.8
Functionality	3.9	3.6	3.42	3.13
%Relative crosslink density	100	94.2	86.8	69.7
Isocyanate Index	1.1	1.1	1.1	1.1

To eliminate the influence of other variables, the isocyanate index was fixed at 1.1 for all recipes, and identical amounts of catalysts, surfactant, and water were used. Furthermore, each formulation was foamed at four different cyclopentane loadings (8, 10, 12, and 14 g), enabling the generation of a range of densities suitable for subsequent density normalization. This approach provided a robust dataset to isolate the effect of crosslink density on compressive strength and modulus.

Theoretically, increasing crosslink density enhances the rigidity of the polymer network, as more three-dimensional connections between polymer chains restrict molecular mobility and reinforce the structural framework. As a result, foams with higher crosslink density are expected to exhibit improved resistance to compressive deformation, manifested as higher compressive strength and modulus.

Figures 8 and **9** display the normalized compressive strength and compressive modulus, respectively, for all four crosslink density formulations, evaluated at the reference density of 40 kg/m³. The data show a clear, monotonic increase in both mechanical properties with

DOI: https://doi.org/10.17509/ajse.v6i1.89937
p- ISSN 2776-6098 e- ISSN 2776-5938

increasing crosslink density. This trend provides strong empirical support for the theoretical prediction that enhanced network connectivity translates into improved mechanical integrity under load.

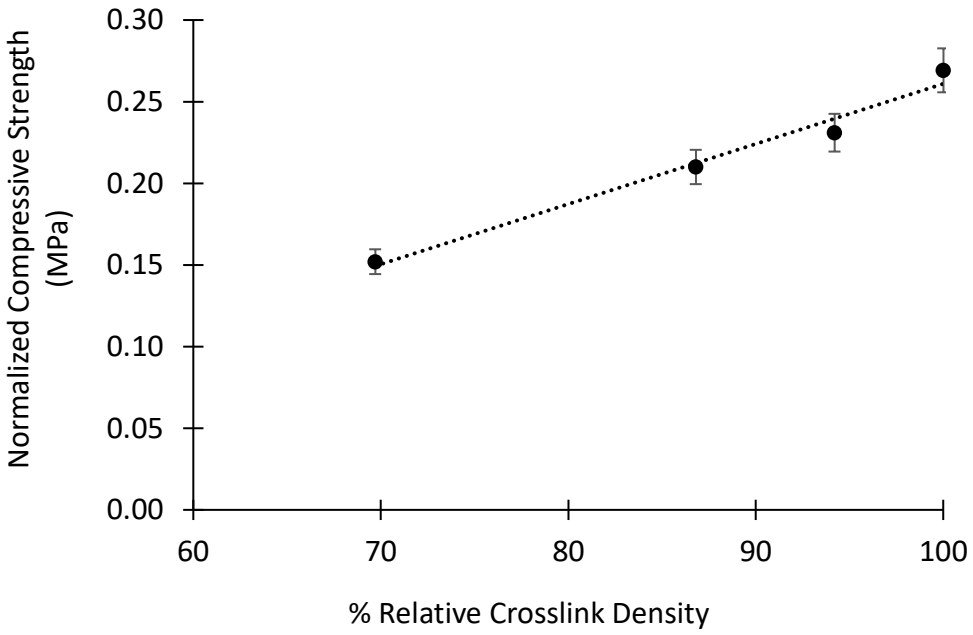

Figure 8. Impact of relative crosslinked density on the normalized compressive strength.

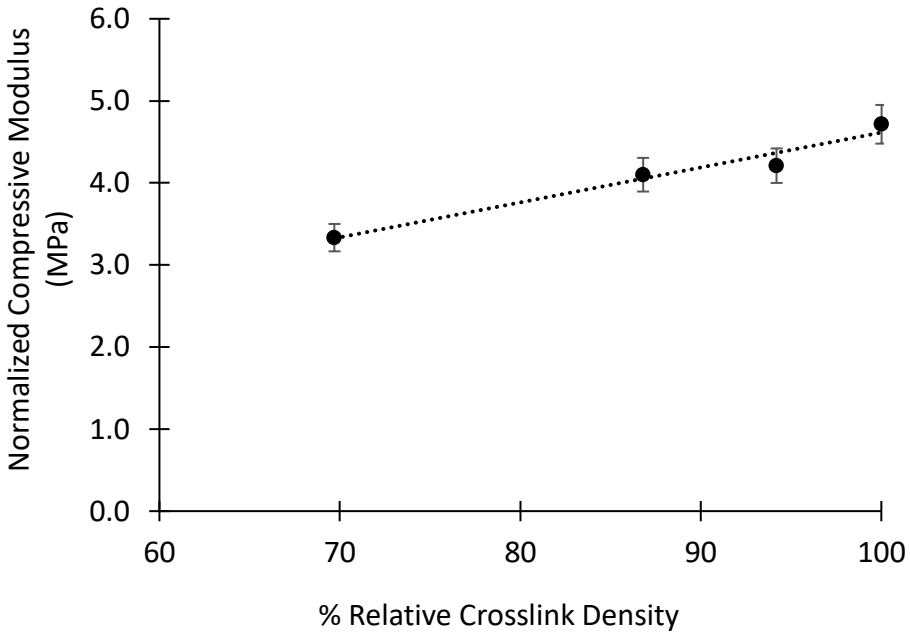

Figure 9. Impact of relative crosslinked density on the normalized compressive modulus.

This relationship highlights the critical role of crosslink density in tailoring RPUF performance. As the formulation shifts toward higher polyol functionality, the resulting foam becomes more structurally rigid, offering greater compressive resistance. Such behavior is highly desirable in applications where dimensional stability and load-bearing capability are essential, including construction panels, impact-absorbing materials, and thermally insulating structural components.

DOI: https://doi.org/10.17509/ajse.v6i1.89937
p- ISSN 2775-6793 e- ISSN 2775-6815

The findings also validate the effectiveness of the normalization methodology adopted in this study, as it allows for clear differentiation between formulation effects while controlling for density variations. In the following discussion, additional considerations such as foam shrinkage at low crosslink density are addressed to contextualize limitations and edge behaviors in the dataset.

Foams formulated with the lowest relative crosslink density (69.7%) exhibited substantial shrinkage when produced with high cyclopentane loading (14 g). This collapse behavior is attributed to the insufficient structural rigidity of the polymer matrix, which was unable to withstand the internal vacuum pressure generated as volatile gases within the cells condensed during cooling. Inadequate crosslinking likely resulted in poor cell wall reinforcement, allowing atmospheric pressure to compress the foam structure.

Due to the severe deformation observed, these samples were excluded from compressive testing, as their compromised geometry rendered an accurate mechanical evaluation impossible. To maintain the continuity of the data set and enable comparative analysis, the normalized compressive properties for the formulation with 73% relative crosslink density were extrapolated from the available data obtained from higher crosslink density formulations. This extrapolation was performed using established trends in the normalized dataset and allowed meaningful insights to be retained despite the limitations imposed by sample shrinkage.

3.4. Effect of Index

The influence of the isocyanate index on compressive behavior was explored using foam formulations R3-1 through R3-5, in which the index was systematically varied from 1.0 to 1.4. All other formulation components (including polyol content, catalysts, surfactant, water, and cyclopentane) were held constant, ensuring that any observed effects could be attributed solely to changes in the isocyanate-to-hydroxyl ratio.

The results of this investigation are shown in **Figures 10** and **11**, which present the density-normalized compressive strength and modulus, respectively, as functions of isocyanate index. In addition, **Figure 12** illustrates the variation in glass transition temperature (Tg), determined via dynamic mechanical analysis (DMA), with increasing index.

The mechanical data reveal that increasing the isocyanate index led to only modest changes in normalized compressive strength and modulus. Although a slight upward trend was observed, the differences were not substantial within the studied range. In contrast, a clear increase in Tg was noted with higher isocyanate indices, indicating a denser crosslinked network and reduced polymer chain mobility.

These findings suggest that while crosslink density (as modulated by the isocyanate index) does affect thermal transitions, it may have a limited impact on compressive performance under room temperature conditions. One possible explanation lies in the relaxation behavior of the polymer matrix: although increased crosslinking can stiffen the foam, it may not significantly enhance its ability to resist compressive loads without concurrent changes in foam density or cell morphology.

This highlights a critical insight: enhancing compressive strength through crosslinking alone has diminishing returns beyond a certain threshold. To achieve further improvements in mechanical performance, a holistic optimization strategy is necessary, one that considers not only chemical structure (e.g., index and crosslink density) but also physical structure, such as cell size, cell anisotropy, and overall foam density.

DOI: https://doi.org/10.17509/ajse.v6i1.89937
p- ISSN 2776-6098 e- ISSN 2776-5938

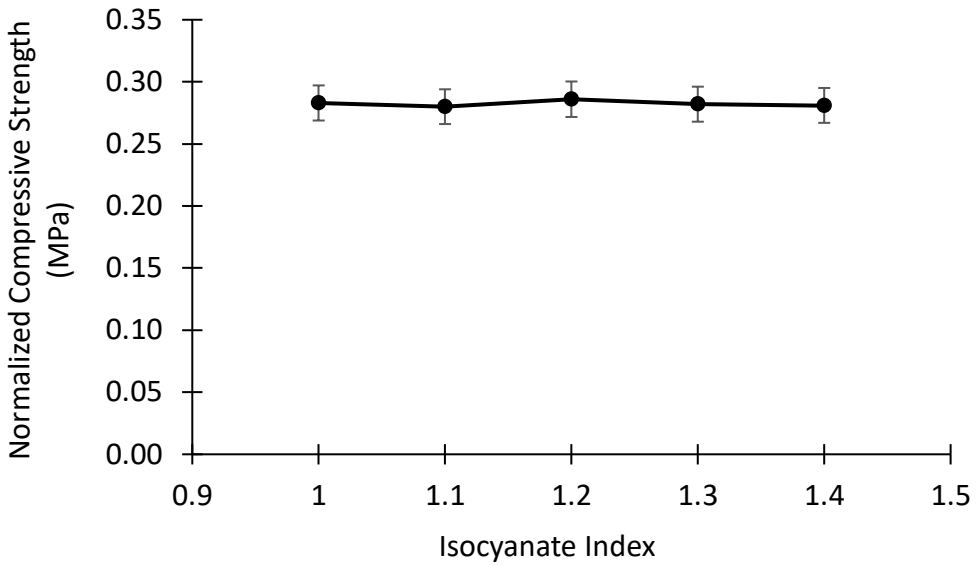

Figure 10. Impact of the isocyanate index on the normalized compressive strength.

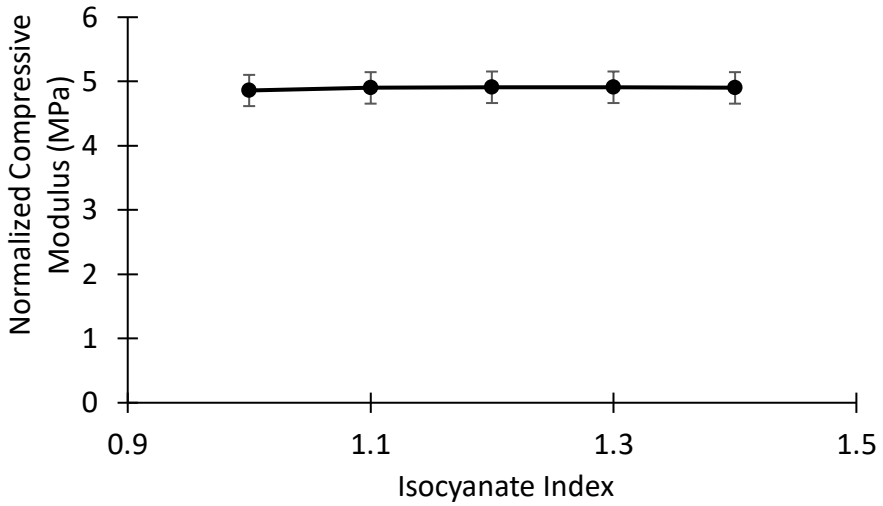

Figure 11. Impact of the isocyanate index on the normalized compressive modulus.

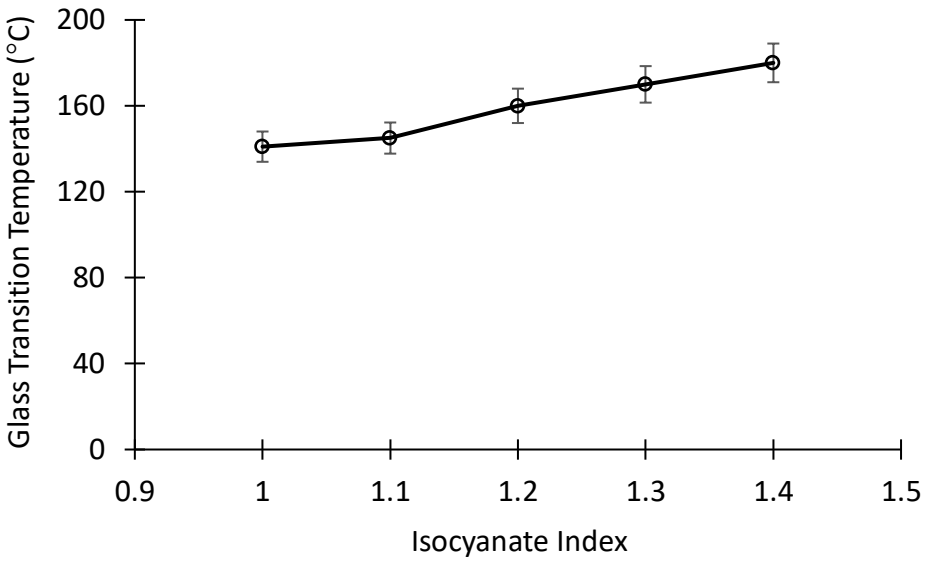

Figure 12. Impact of the isocyanate index on the glass transition temperature.

DOI: https://doi.org/10.17509/ajse.v6i1.89937
p- ISSN 2775-6793 e- ISSN 2775-6815

4. CONCLUSIONS

The compressive strength of RPUF is essential for ensuring its functionality in a wide range of applications, particularly when used as load-bearing materials. This mechanical property directly influences the capacity of the foam to endure compressive forces without succumbing to deformation or failure. RPUF is utilized in diverse fields, including packaging and insulation, where its mechanical properties are pivotal. This study investigated the compressive characteristics of various PU recipes using a normalization approach. Standardizing the foam samples to a consistent foam density facilitated a balanced comparison method. The key parameters examined during the investigation included foam density, aging, crosslink density, and isocyanate index, with a specific focus on foam. Five distinct cyclopentane concentrations were subjected to controlled environmental conditions, with a relative humidity of 50% and a temperature of 24°C. The normalization process enabled the evaluation of the compressive strength and modulus at a unified density. Over this period, a notable reduction of approximately 31.6% in the normalized compressive strength was documented, whereas the compressive modulus exhibited an increase of approximately 63.8%. A higher crosslink density contributed significantly to enhanced foam rigidity, which was attributed to the reinforced material structure. However, minimal changes were observed in the normalized compressive strength and modulus as the isocyanate index increased. Despite this, foams with elevated isocyanate indices demonstrated a higher glass transition temperature, indicating that an increased crosslink density had been successfully achieved. The influence of crosslink density on foam properties appears to stem from the relaxation behavior that is inherent to the polymer matrix. These findings provide valuable insights into the interplay of foam density, aging, crosslink density, and isocyanate index in determining the mechanical performance of RPUF, paving the way for potential applications in optimizing RPUF for enhanced durability in construction insulation, automotive components, and aerospace structures, where reliable load-bearing capabilities are critical.

5. ACKNOWLEDGMENT

This study is supported by Mustansiriyah University (www.uomustansiriyah.edu.iq) and Al-Naji University, Baghdad-Iraq.

6. AUTHORS' NOTE

The authors declare that there is no conflict of interest regarding the publication of this article. The authors confirmed that the paper was free of plagiarism.

7. REFERENCES

[1] Nandiyanto, A.B.D., Ragadhita, R., and Fiandini, M. (2023). Interpretation of Fourier Transform Infrared Spectra (FTIR): A practical approach in the polymer/plastic thermal decomposition. *Indonesian Journal of Science and Technology*, *8*(1), 113-126

[2] Sridevi, V., Hamzah, H.T., Jweeg, M.J., Mohammed, M.N., Al-Zahiwat, M.M., Abdullah, T.A., and Abdullah, O.I. (2024). Microwave pyrolysis of agricultural and plastic wastes for production of hybrid biochar: Applications for greener environment. *Indonesian Journal of Science and Technology, 9*(3), 791-820.

[3] Sarkingobir, Y., and Tukur, U. (2025). Plastic in water and its implications in human and biological systems. *ASEAN Journal for Science and Engineering in Materials*, *4*(1), 1-12.

DOI: https://doi.org/10.17509/ajse.v6i1.89937
p- ISSN 2776-6098 e- ISSN 2776-5938

[4] Samsuri, S., Anwar, S., Harini, S., Kartini, T., Monaya, N., Warizal, W., and Setiawan, A.B. (2025). Techno-economic feasibility and bibliometric literature review of integrated waste processing installations for sustainable plastic waste management. *ASEAN Journal for Science and Engineering in Materials*, *4*(2), 225-244.
[5] Cao, Z., Hao, Q., Xu, S., Han, X., Yi, J., and Sun, G. (2025). Preparation and performance evaluation of bio-based polyurethane modified asphalt binders: Towards greener and more sustainable asphalt modifier. *Construction and Building Materials, 476*, 141209.
[6] Mohammed, A.J., Muhsen, M.C., and Ibrahim, I.K. (2023). Effect of additional natural filler waste on the mechanical properties of polyurethane polymer. *ASEAN Journal for Science and Engineering in Materials*, *2*(2), 135-142.
[7] Zhai, D., Sun, Q., Wang, Y., and Li, J. (2024). Microstructure and mechanical performance of polyurethane-fly ash composites (PU-FAC) under different effect factors. *Case Studies in Construction Materials, 21*, e03405.
[8] Lu, P., He, C., Wang, J., Wu, Y., and Ding, J. (2025). Polyurethane-modified asphalt mechanism. *Case Studies in Construction Materials, 22*, e04247.
[9] Sun, C., Bu, X., Yang, T., Qiao, C., Ji, X., Tao, F., and Liu, L. (2023). Degradable waterborne polyurethane with flame retardancy and high mechanical strength via synergy of hydrogen bonds. *ACS Applied Polymer Materials*, *5*(7), 5360-5369.
[10] Wang, S., Liu, W., Yang, D., and Qiu, X. (2019). Highly resilient lignin-containing polyurethane foam. *Industrial and Engineering Chemistry Research, 58*(1), 496–504.
[11] Benavides, S., Armanasco, F., Cerrutti, P., and Chiacchiarelli, L. M. (2021). Nanostructured rigid polyurethane foams with improved specific thermo-mechanical properties using bacterial nanocellulose as a hard segment. *Journal of Applied Polymer Science, 138*(22), 50520.
[12] Hu, Z.-Q., Shao, J.-L., and Chen, P.-W. (2024). The effect of silica nanoparticles on the shock adiabatic relation and tensile strength in polyurethane. *Mechanics of Materials, 192*, 104979.
[13] Wei, W., Bi, Y., and Bi, G. (2023). Study of viscoelastic damage and micromechanism of polyurethane in freeze-thaw cycle environment. *Case Studies in Construction Materials, 19*, e02551.
[14] Cortazar-Noguerol, J., Cortés, F., and Elejabarrieta, M. J. (2025). Influence of density of a polyurethane microcellular elastomer foam on its compressive energy absorption and time-dependent behavior. *Journal of Materials Research and Technology, 34*, 439–448.
[15] Jung, H. C., Ryu, S. C., Kim, W. N., Lee, Y.-B., Choe, K. H., and Kim, S.-B. (2001). Properties of rigid polyurethane foams blown by HCFC 141B and distilled water. *Journal of Applied Polymer Science, 81*(2), 486–493.
[16] Sarkari-Oskuei, E., Safavi-Mirmahalleh, S.-A., Sofla, R. L. M., Roghani-Mamaqani, H., and Salami-Kalajahi, M. (2023). Synthesis of recyclable polyurethane-based pseudo-vitrimer: Comparison of properties with conventional polyurethane. *Journal of Polymer Research, 30*(9), 338.
[17] Harikrishnan, G., Patro, T. U., and Khakhar, D. V. (2006). Polyurethane foam–clay nanocomposites: Nanoclays as cell openers. *Industrial and Engineering Chemistry Research, 45*(21), 7126–7134.
[18] Kantheti, S., Narayan, R., and Raju, K. V. S. N. (2014). Click chemistry engineered hyperbranched polyurethane-urea for functional coating applications. *Industrial and Engineering Chemistry Research, 53*(20), 8357–8365.

DOI: https://doi.org/10.17509/ajse.v6i1.89937
p- ISSN 2775-6793 e- ISSN 2775-6815

[19] Su, Y., Tian, J., and Zhang, H. (2025). The role of compressive stress enhancement in the shear mechanism of nickel foam/polyurethane composites. *Composites Part A: Applied Science and Manufacturing, 190*, 108699.
[20] Omrani, I., and Mohammadi Berenjegani, R. (2024). Chemical recycling of flexible polyurethane foam scraps using bio-based acidolysis agents. *ACS Applied Polymer Materials, 6*(17), 10698–10705.
[21] Zhai, D., Sun, Q., Liu, Z., and Yue, X. (2025). Study on the pore characteristics of polyurethane-based repair materials. *Construction and Building Materials, 483*(7), 141058.
[22] Huang, W., Xu, H., Fan, Z., Ao, Y., and Liu, J. (2020). Compressive response of composite ceramic particle-reinforced polyurethane foam. *Polymer Testing, 87*, 106514.
[23] Xu, Z., Fan, Y., Tao, P., Wang, L., Wang, C., Guo, X., and Quan, Y. (2024). Multimethod recyclable thermoset polybutadiene polyurethane-urea via reversible disulfide bonds. *ACS Applied Polymer Materials*, *6*(10), 6183-6191.
[24] Pengfei, L., Jie, W., Zhilong, C., Jian, X., Song, L., Peng, W., and Zhiqing, Z. (2025). Degradation mechanism and performance of polyurethane mixture under water conditions. *Construction and Building Materials*, *490*, 142467.
[25] Yuan, H., Wang, Y., Liu, Z., and Li, S. (2019). A study on the properties and working mechanism of a waterborne polyurethane-modified silicate-based coating. *RSC Advances, 9*(46), 26817–26824.
[26] Yang, F., Gao, H., Jiang, J., Wang, M., and Hu, G. (2023). Influence of microphase separation and crosslinking density on dynamic viscoelastic properties of nano-FeO modified polyurethane. *Journal of Applied Polymer Science, 140*(41), e54521.
[27] Ma, P., Ma, L., Wang, M., Duan, L., Tan, Y., and Zhu, W. (2024). Compressive strength characteristics of polyurethane cemented sea sand. *Case Studies in Construction Materials, 20*, e03172.
[28] Husainie, S. M., Khattak, S. U., Robinson, J., and Naguib, H. E. (2020). A comparative study on the mechanical properties of different natural fiber reinforced free-rise polyurethane foam composites. *Industrial and Engineering Chemistry Research, 59*(50), 21745–21755.
[29] Soares, L. F., dos Santos, J. C., de Freitas, V. A. A., Pereira, R. B. D., Panzera, T. H., and Scarpa, F. (2024). Castor-oil biobased foam: The effect of the composition on the physical and mechanical properties via a statistical mixture design. *RSC Sustainability, 2*(4), 975–987.
[30] Sajadian, Z., Zebarjad, S. M., and Bonyani, M. (2024). Thermal and mechanical properties of honeycomb sandwich panel of polyurethane nanocomposite reinforced with nanoclay. *Journal of Polymer Research, 31*(9), 284.
[31] Akhtar, A. Y., and Tsang, H.-H. (2023). Dynamic properties of recycled polyurethane-coated rubber-soil mixtures. *Case Studies in Construction Materials, 18*, e01859.
[32] Zhang, Q., Hu, X., Ma, H., Li, W., and Jin, X. (2024). Aging behavior of polyether polyurethane binder: Thermal-oxidative, photo-oxidative, hydrolytic aging, and microscale. *Construction and Building Materials, 455*, 139077.
[33] Zhang, S., Wang, R., Du, Y., Liu, J., Hu, X., Xu, M., and Li, B. (2025). Inherently flame retardant and aging resistance rigid polyurethane foam by incorporating the synthesized polyhydroxy phosphonates. *Composites Communications*, *53*, 102246.
[34] Wang, L., Xiang, S., Ling, G., Ying, J., Zhou, J., and Yang, J. (2025). New modification strategy for thermoplastic polyurethane with high hygrothermal ageing resistance and flame retardancy. *Polymer Degradation and Stability*, *232*, 111140.

DOI: https://doi.org/10.17509/ajse.v6i1.89937
p- ISSN 2776-6098 e- ISSN 2776-5938

[35] Wang, L., O'Connor, D., Rinklebe, J., Ok, Y. S., Tsang, D. C., Shen, Z., and Hou, D. (2020). Biochar aging: mechanisms, physicochemical changes, assessment, and implications for field applications. *Environmental Science and Technology*, *54*(23), 14797-14814.
[36] Yarahmadi, N., Vega, A., and Jakubowicz, I. (2017). Accelerated ageing and degradation characteristics of rigid polyurethane foam. *Polymer Degradation and Stability, 138*, 192–200.
[37] Malucelli, G. (2025). Flame retardant surface treatments for rigid polyurethane foams used in the building sector: Current state-of-the-art and perspectives. *Construction and Building Materials, 472*(4), 140947.
[38] Davies, P., and Evrard, G. (2007). Accelerated ageing of polyurethanes for marine applications. *Polymer Degradation and Stability, 92*(8), 1455–1464.
[39] Labouriau, A., Stockdale, J. R., Adhikari, S., Pacheco, A., Legett, S. A., Davis, J., and Torres, X. M. (2024). Suitability of aromatic polyurethanes for use in nuclear applications. *Polymer Degradation and Stability*, *228*, 110920.
[40] Campos, G. N., Coimbra, A. C. R., Silva, A. A. D., Rocha, E. B. D. D., Linhares, F. N., Furtado, C. R. G., and Sousa, A. M. F. D. (2022). Cross-link density measurement of nitrile rubber vulcanizates using dynamic shear test. *Polímeros*, *32*, e2022011.
[41] Chiou, B.-S., and Schoen, P. E. (2002). Effects of crosslinking on thermal and mechanical properties of polyurethanes. *Journal of Applied Polymer Science, 83*(1), 212–223.
[42] Song, J., Wu, H., Niu, Y., Hui, B., Wang, Y., and Li, L. (2024). Modification of degradable polyurethane materials using L-tyrosine and its application. *Journal of Polymer Research, 32*(1), 15.
[43] Kumar, R., Liu, D., and Zhang, L. (2008). Advances in proteinous biomaterials. *Journal of Biobased Materials and Bioenergy*, *2*(1), 1-24.
[44] Al-Moameri, H., Jaf, L., and Suppes, G. J. (2021). Simulation approaches for the mechanisms of thermoset polymerization reactions. *Molecular Catalysis*, *504*, 111485.
[45] Merillas, B., Lamy-Mendes, A., Villafañe, F., Durães, L., and Rodríguez-Pérez, M. Á. (2022). Polyurethane foam scaffold for silica aerogels: Effect of cell size on the mechanical properties and thermal insulation. *Materials Today Chemistry, 26*, 101257
[46] Fu, Y., Qiu, C., Ni, L., Ye, H., Zou, H., Luo, Y., and Liang, M. (2024). Cell structure control and performance of rigid polyurethane foam with lightweight, good mechanical, thermal insulation and sound insulation. *Construction and Building Materials*, *447*, 138068.
[47] Wang, H., Xie, S., Jing, K., Zheng, S., Liu, Z., and Zhou, H. (2025). Closed-cell polyurethane in-situ foaming honeycomb for enhanced energy absorption and water intrusion resistance. *Alexandria Engineering Journal, 114*, 572–587.
[48] Singh, D., and Ohri, S. (1982). Effect of reactant ratio and temperature on the characteristics of phenol–formaldehyde foams. *Journal of Applied Polymer Science, 27*(4), 1191–1196.
[49] Masi, P., Nicolais, L., Mazzola, M., Snial, and Narkis, M. (1983). Tensile properties of fiberglass-reinforced polyester foams. *Journal of Applied Polymer Science, 28*(4), 1517–1525.
[50] Hoseinabadi, M., Naderi, M., Najafi, M., Motahari, S., and Shokri, M. (2017). A study of rigid polyurethane foams: The effect of synthesized polyols and nanoporous graphene. *Journal of Applied Polymer Science, 134*(26), 45001.
[51] Krumova, M., López, D., Benavente, R., Mijangos, C., and Pereña, J. M. (2000). Effect of crosslinking on the mechanical and thermal properties of poly(vinyl alcohol). *Polymer*, *41*(26), 9265–9272.

DOI: https://doi.org/10.17509/ajse.v6i1.89937
p- ISSN 2775-6793 e- ISSN 2775-6815

[52] Golker, K., and Nicholls, I. A. (2016). The effect of crosslinking density on molecularly imprinted polymer morphology and recognition. *European Polymer Journal, 75*, 423–430.

[53] Iezzi, E. B., Daniels, G. C., Sutyak, K., and Camerino, E. (2024). Impact of cross-linker structure on the properties of durable and selectively degradable silyl-containing polyurethane networks. *ACS Applied Polymer Materials, 6*(14), 8178–8190.

[54] Andersons, J., Cabulis, P., and Kirpluks, M. (2022). The effect of crosslink density on the physical and mechanical properties of bio-based polyurethane foams. *Macromolecular Symposia, 404*(1), 2100329.

[55] Nabeth, B., Corniglion, I., and Pascault, J. P. (1996). Influence of the composition on the glass transition temperature of polyurethane and polyurethane acrylate networks. *Journal of Polymer Science Part B: Polymer Physics, 34*(3), 401–417.

[56] Li, S., Vatanparast, R., Vuorimaa, E., and Lemmetyinen, H. (2000). Curing kinetics and glass-transition temperature of hexamethylene diisocyanate-based polyurethane. *Journal of Polymer Science Part B: Polymer Physics, 38*(17), 2213–2220.

DOI: https://doi.org/10.17509/ajse.v6i1.89937
p- ISSN 2776-6098 e- ISSN 2776-5938